PROCEEDINGS OF SPIE

Rapid detection of intact SARS-CoV-2 viral particles using silicon nanomembranes

Klaczko, Michael, Ozgurun, Baturay, Ward, Brian, Flax, Jonathan, McGrath, James

SPIE.

Rapid detection of intact SARS-CoV-2 viral particles using silicon nanomembranes

Michael Klaczko[a], Baturay Ozgurun[b], Brian Ward[c], Jonathan Flax[d], and James McGrath*[b]

[a]Department of Chemistry, University of Rochester, Rochester, NY, USA 14627; [b]Department of Biomedical Engineering, University of Rochester, Rochester, NY, USA 14627; [c]Department of Microbiology and Immunology, University of Rochester Medical Center, Rochester, NY, USA 14642; [d]Department of Urology, University of Rochester Medical Center, Rochester, NY, USA 14642

ABSTRACT

The SARS-CoV-2 pandemic has revealed the need for rapid and inexpensive diagnostic testing to enable population-based screening for active infection. Neither standard diagnostic testing, the detection and measurement of viral RNA (via polymerase chain reaction), or serological testing (via enzyme-linked immunosorbent assay) has the capability to definitively determine active infection. The former due to a lack of ability to distinguish between replicable and inert viral RNA, and the latter due to varying immune responses (ranging from latent to a complete lack of immune response altogether). Despite many companies producing rapid point-of-care (POC) tests, none will address the global scale of testing needed and few help to combat the ever growing issue of testing resource scarcity. Here we discuss our efforts towards the development of a highly manufacturable, microfluidic device that instantly indicates active viral infection status from ~ 20 μL of nasal mucus or phlegm and requires no external power. The device features a biotin functionalized silicon nanomembrane within an acrylic body containing channels and ports for sample introduction and analysis. Virus capture and target confirmation are done using affinity-based capture and size-based occlusion respectively. Modularity of the device is proven with bead and vaccinia virus capture as we work towards testing with both pure SARS-CoV-2 virus and human samples. With success on all fronts, we could achieve an inexpensive POC diagnostic which can determine an individual's infection status, aiding containment efforts in the current and future pandemics. In addition to direct viral detection, our method can be used as a rapid POC sample preparation tool that limits the application of PCR reagents to those samples which already display viral size and antigen-based positivity through our device.

Keywords: nanotechnology, high resolution imaging, membrane, point-of-care, diagnostics, microfluidics

1. INTRODUCTION

While the scale of the SARS-CoV-2 pandemic is not unprecedented, the global response has been and signals a new societal expectation that public health sectors should be prepared to quickly control the spread of deadly infectious disease. While great advances in technology and healthcare underly this expectation and have in fact performed with historic speed and effectiveness, current shortcomings are evident, discussed daily, and will remain the focus of research and progress for decades to come. One continuing area of focus will be in POC testing that provides more complete information about a patient's status with respect to the course of infection. In particular the detection of long-lived RNA fragments postulated to circulate long after a patient is symptomatic or infectious[1-4] have likely caused undue anxiety and productivity losses.

1.1 Current Testing Capabilities

Available testing for SARS-CoV-2 can be broken up into two main categories: serological testing and diagnostic testing[5]. Serological testing detects antibodies created in response to viral exposure, while diagnostic testing detects viral RNA or viral antigens. Both categories can be further broken down into laboratory benchtop testing and rapid POC tests. The gold standard in both techniques are the laboratory benchtop techniques enzyme-linked immunosorbent assays (ELISA) and polymerase chain reaction (PCR), respectively. The established prominence of both techniques in diagnostics allowed for their immediate and continued use for detection of immunity and infectious spread of SARS- CoV-2[6,7,8]. Despite their

*jmcgrath@bme.rochester.edu; phone 1 585 273-4746; fax 1 585 273-4746; www.urmc.rochester.edu/labs/mcgrath.aspx

success, continued spread of the virus spurred greater testing demands, ultimately resulting in a greater interest in rapid POC diagnostics[9]. Towards this effort many tests have been developed for both serology and diagnostic applications[10]. For serology testing lateral flow assays, chemiluminescence assays, electrochemiluminescence assays, fluorescent microsphere immunoassays, and chemiluminescent microparticle assays among others were developed. For diagnostic testing reverse transcription loop-mediated isothermal amplification (RT-LAMP), isothermal reverse transcriptase helicase dependent amplification (RT-HDA), reverse transcriptase-isothermal amplification, and lateral flow assays of all three and more were developed. While these tests filled the growing demand for rapid testing, few performed as well as their respective gold standard diagnostics[11-16]. In addition, none of these or the gold standard tests have provided the increasingly important ability to reliably determine an individual's infection status[5,17,18]. In response to this gap in testing ability, we have directed our technology towards the detection of intact virus in biofluids. Our approach has the potential to be used as a stand-alone POC test or in combination with POC molecular tests.

1.2 Microfluidic sensor design and the 'resistance switch'

Ultrathin, silicon-based nanomembranes were introduced by the McGrath lab in 2007 and have been successfully used in various microfluidic applications since[19-23]. To create a virus capture sensor, we used a multi-layered microfluidic assembly developed in collaboration with ALine Inc. This device was first used as a cell culture and modeling platform, but the single input to dual output design allowed for its easy adoption as a sensing platform[24,25]. Our concept, visually represented in Figure 1a and 1b, was to use the device to create a simple fluidic bifurcation in which one fluid path is selected in the presence of virus and a second fluid path is selected in the absence of virus. From previous work we knew we could make a switch between fluid paths by using our nanomembrane as a fouling-based variable resistor[19,21,23,26]. Thus we designed the device so that clean fluid would prefer a path through the nanomembrane by ensuring this path initially had the lowest resistance of the two flow paths. However, if the pores of the membrane become occluded due to the capture of virus, the low resistance path becomes closed and flow is routed to the second path. In this way nanomembranes are used as a 'resistance switch' that distinguishes between a positive and negative sample. Designed as a diagnostic test, we refer to these new devices as μSIM-DX (**micro**fluidic device featuring a **si**licon **m**embrane for **d**iagnos**t**ics).
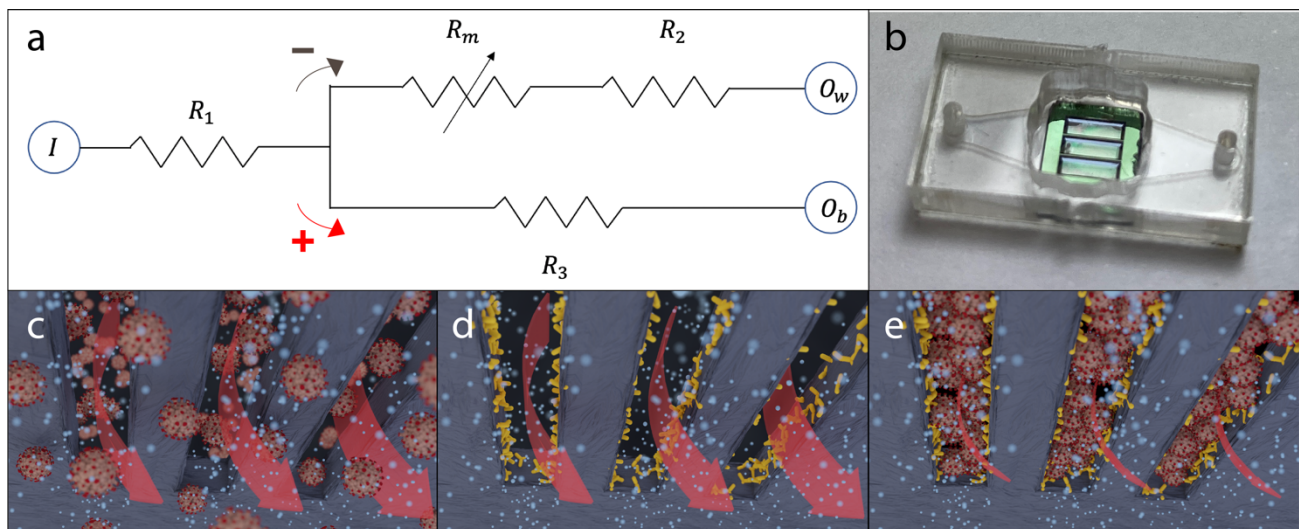

Figure 1. From concept to prototype design, the development of the microfluidic sensor is shown as a microfluidic circuit schematic (a). I represents the μSIM-DX inlet and R_1 represents the initial channel resistance. The path of least resistance goes up through the membrane and top channel whose resistances are represented by R_m and R_2 respectively and out the outlet of the well, O_w. The bottom path is chosen and fluid exits the bottom channel outlet, O_b, as the resistance of the upper path becomes greater than the bottom path resistance, R_3. The completed microfluidic sensor is shown in (b). Within the sensor an uncoated microslit membrane will allow SARS-CoV-2 to pass through uncaptured (c) while a Kode[TM]-biotin coated membrane (d) will not, capturing streptavidin conjugated antibody-bound virus via affinity-based capture (e).

1.3 Membrane functionalization using amphiphilic molecules

Traditionally we have used nanomembranes to filter or capture targets based on their size[19,21,23,26]. This means that any pore occlusion would occur via steric capture, shown in Figure 1c. While this approach works well for simple solutions, complex mixtures such as biofluids and smaller targets would benefit from the specificity of antibody-based capture. In the current application we functionalize the membranes with amphiphilic molecules, made by Kode Biotech Ltd. These molecules have a hydrophobic lipid tail, a hydrophilic spacer, and a functional head group[27,28]. The silicon composition of our membrane offers a slightly hydrophobic surface which coordinates with the hydrophobic tails of Kode[TM]. To create a facile linking system, we utilize a Kode[TM] molecule variant which has a biotin functional head group, hereafter referred to as 'Kode[TM] -biotin'.

1.4 Affinity-based capture

With biotin presenting on the surface of our nanomembranes after functionalization with Kode[TM]-biotin, we sought to take advantage of the robust biotin-avidin linker system to capture virus. Since its discovery over 40 years ago, the biotin-avidin system has been shown to provide quick interactions and bind stronger than any known non-covalent bond29. To apply this system to virus capture, we streptavidin-conjugated antibodies raised against surface glycoproteins on the virus surface. In the case of SARS-CoV-2 these antibodies recognize the spike proteins that give the corona virus its name. In the case of vaccinia virus, the antibodies recognize L1 surface transmembrane proteins. Illustrated in Figure 1d-e, our strategy allows us to pre-mix streptavidin conjugated antibody with sample and inject the mixture into the μSIM-DX where the virus-antibody-streptavidin complex will be captured on the biotin coated membrane if the virus is present. Even if unbound streptavidin conjugated antibody or streptavidin conjugated antibody bound to free floating virus proteins are captured on the membrane, a resistance switch will not be triggered as only the virus is sufficient to occlude pores and cause a switch. Thus, our sensor has a unique requirement for simultaneous size and antigen-based recognition of the virus. We have established proof-of-principle with streptavidin conjugated beads and vaccinia virus as surrogates upstream of SARS-CoV-2.

1.5 Capture analysis using fluorescence microscopy

To quantify the sensitivity of fouling-based sensing, we used fluorescence microscopy of membranes following the capture of fluorescently labeled particles and virus. Given the size of the targets that we are capturing (beads – 200 nm/500 nm, vaccinia virus – 300 nm, SARS-CoV-2 – 65-125 nm), high resolution microscopy will be necessary for direct quantification by counting[30,31]. For our study we used both a Leica DMIRB inverted fluorescence microscope and an Andor Dragonfly spinning disc confocal microscope.

2. METHODOLOGY

2.1 Membrane functionalization

Microslit membranes (0.5 μm slit-pore) silicon nanomembranes were purchased from SiMPore Inc. (West Henrietta, NY). These chips were subsequently cleaned with a piranha solution (3:1 H_2SO_4:H_2O_2) for 30 minutes and rinsed thoroughly with deionized water. Kode[TM]-biotin amphiphilic molecules were purchased from Kode Biotech Ltd. (Auckland, New Zealand). 12.5 μM solutions were made in 70% ethanol. The cleaned membranes were submerged in the Kode[TM] solutions for 1 minute under gentle agitation. These membranes were then removed and heated in a 65°C oven for 40 minutes. After heating the membranes are rinsed in 70% ethanol and allowed to dry.

2.2 μSIM-DX fabrication

Acrylic microfluidic components and device assembly jigs were purchased from ALine Inc. (Rancho Dominguez, CA). μSIM-DXs were assembled by applying pressure to acrylic components lined with pressure sensitive adhesive onto our functionalized membranes with the aid of the assembly jigs. Modifications were made using a drill press and different sized PEEK tubing ordered from LabSmith Inc. (Livermore, California). Tubes were sealed into the μSIM-DX using polymer sealant.

2.3 Sample testing

Fluorescent streptavidin conjugated polymer beads (200 nm and 500 nm exc/em-480 nm/520 nm) were purchased from Bangs Laboratories Inc. (Fishers, IN). Ethanol fixed mKate2 (exc/em-588 nm/633 nm) labelled vaccinia virus and vaccinia virus antibody were provided by our medical center collaborator, Dr. Brian Ward. Solutions were made in PBS and stored at 4°C if necessary. The vaccinia antibody was streptavidin conjugated using the protocols and reagents provided by the Streptavidin Conjugation Kit – Lightning Link® from abcam (Cambridge, MA). Conjugated antibody was pre-mixed with vaccinia to ensure ample antibody-protein interaction time. μSIM-DX bottom channels and wells were pre-wet with PBS if appropriate. Samples were injected by hand using standard P200 pipettes.

2.4 Fluorescence and confocal microscopy

Fluorescence microscopy was done using a Leica DMIRB inverted fluorescence microscope with a halogen lightbulb and filter cube setup and a charge-coupled-device camera. Confocal microscopy was completed on an Andor Dragonfly Spinning Disc Confocal microscope with a Zyla 4.2 sCMOS camera. Chips were left in their μSIM-DXs and imaged after testing. A 488 nm laser was used to excite the fluorescent beads and a 500 nm filter was used to capture emission. A 561 nm laser was used to excite the mKate2 labeled vaccinia virus and a 600 nm filter was used to capture emission.

3. RESULTS

3.1 μSIM-DX performance

Testing with bead and vaccinia virus allowed us to safely establish proof-of-concept and optimize the μSIM-DX prior to SARS-CoV-2 studies. Shown in Figure 2, initial testing with blank solutions of PBS did not trigger a resistance switch, while 10E5 bead/mL solutions of both 500 nm beads (steric capture) and 200 nm (affinity capture) streptavidin coated beads did trigger a resistance switch. Confocal imaging of bead capture reveals widespread bead capture for both sizes, confirming the ability of the μSIM-DX to capture targets based on size or affinity. Widefield fluorescence imaging of vaccinia virus capture also shows widespread virus capture, confirming the sensors ability to capture biological targets and confirming the concept of our pre-mix design. Both 200 nm bead and vaccinia capture also support the use of the biotin-streptavidin linker system which provides an instantaneous method of target capture. To optimize the performance of the μSIM-DX, adjustments can be made to the microfluidic design. Keeping injection flow rates roughly the same, the resistance of the bottom channel can be adjusted to compensate for different volumes or concentrations of bead or vaccinia solutions. Fewer beads or vaccinia means less of the membrane will be occluded, minimizing the resistance change. To account for this, the bottom channel resistance can be lowered by making the channel bigger. The opposite effect can be produced in response to higher concentrations of beads or vaccinia. Through numerous tests with beads and vaccinia virus,
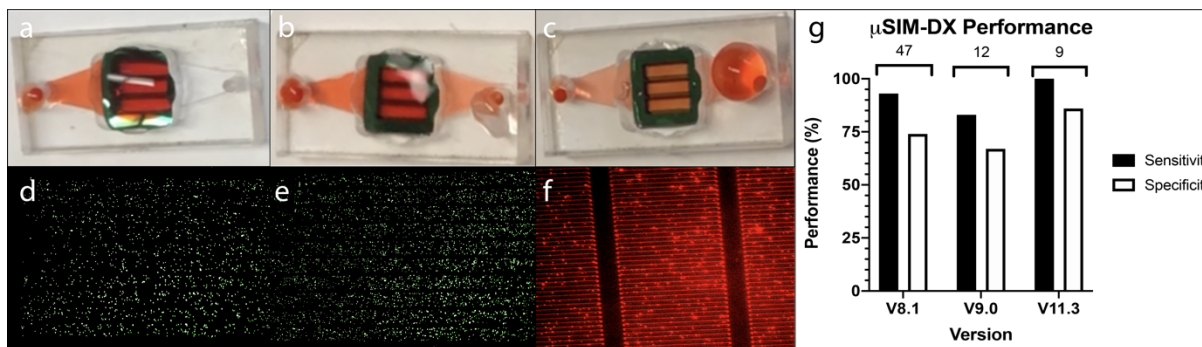

Figure 2. The concept of the μSIM-DX is successfully demonstrated using 40 μL of PBS (a), 500 nm beads (b) and 200 nm streptavidin coated beads (c). In each test red dye was injected afterwards to highlight the path of the injected sample. The PBS injection only makes it to the membrane, while the 500 nm beads and the 200 nm beads occlude then push past the membrane out the outlet port on the right side of the μSIM-DX. Confocal imaging reveals capture of 500 nm beads (d) and 200 nm beads (e) using a 10X objective. Epifluorescence imaging reveals capture of vaccinia virus using a 40X objective (f). Together the combination of bead and vaccinia testing provide the ability to determine μSIM-DX diagnostic sensitivity and specificity, shown for different versions with their n values listed above each version (g).

different device iterations are tracked. Analyzing their performance with true positives/false negatives and true negatives/false positives, their diagnostic sensitivity and specificity can be determined and are also shown in Figure 2. The devices tend to be more sensitive than specific, with sensitivities averaging 92% and specificities averaging 76%.

3.2 Counting using high resolution simulations

Quantifying the number of sub-optical particles captured in fluorescence images will be limited by viral load in samples. Specifically, the resolution of an optical system should determine the maximum concentration of intact virus that can be detected. To explore this limitation, we created synthetic models of particles captured on microslit membranes and simulated wide-field, confocal, and super resolution (stimulated emission depletion or STED) microcopy. To generate an object scene, we first form 30 nanomembrane slits and then release a uniform number of particles per slit. The peak-to-peak distance between two slits is 2 µm, and the dimension of each slit is 50 µm x 0.5 µm. Particles are randomly placed on the inside edge of the slits – simulating affinity-based capture on the pore walls; hence, some particles fully or partially overlap. Excitation and emission wavelengths of the particles are 588 nm and 633 nm, respectively. Once the object is generated, the imaged object is simulated assuming a camera with a 600 x 600 pixel resolution with a pixel pitch of 10 µm, assuming the use of a 100X/1.4NA microscope objective. To create a wide-field image, the object is convolved with a point spread function (PSF). Changing the PSF parameters can allow us to artificially increase the spatial resolution and generate confocal and STED images. The spatial resolution of wide-field, confocal, and STED microscopies are roughly calculated as 226 nm, 199 nm, and 50 nm, respectively. In Figure 3, a simulated wide field nanomembrane image where particles 100 nm in size are randomly placed on each slit, is illustrated. We crop the scene along the white box to demonstrate the particles in detail. The cropped scene image and the corresponding microscope images are shown in the same figure. To evaluate the spatial resolution for the particle counting experiments, we first release a uniform number of particles (between 1 and 100) to each slit and generate corresponding microscope images. We then apply a threshold operation to the microscope images to form binary images and define peak points for each particle. The number of peak points of each particle can be correlated with the number of particles on the membrane. We also repeat the experiments for particles of various sizes (100 nm, 200 nm, and 300 nm). This can allow us to compare the performances of three microscopy modalities for particle counting experiments. In Figure 3, we provided a graph that compares the number of counted particles in percent (the total number of counted particles over the total number of released particles) and the number of released particles per slit. This graph provides data for each microscopy modality (wide-field, confocal, and STED) and each particle size (100 nm, 200 nm, and 300 nm). It is shown that high spatial resolution performs well for the particle counting experiments.

4. DISCUSSION

4.1 Pore occupancy

We note that complete membrane occlusion was not required to trigger a resistance switch indicating the presence of a membrane fouling particle. With 40 µL injections of 10E5 bead/mL or virus/mL solutions, only 4000 beads or virions were being introduced to the membrane. Yet this was enough to cause a resistance switch in most designs of the µSIM-DX. The fact that total pore occupancy had not been achieved was evidenced by the fluorescence microscopy images in Figure 2d-f. More precise control over the point at which the resistance switch occurs could be demonstrated by changing the shape and size of the channels in the µSIM-DX. This could be useful for future applications as the device could be calibrated for different size targets. Adjustments could also be made for infections which require different levels of sensitivity according to their viral loads.

4.2 Pre-mixing to avoid antibody coated membranes

Pre-mixing of antibody with virus, rather than anchoring the antibody to membrane pores, has proven to be an effective approach. In combination with the biotin-streptavidin linker system, we have developed a general approach to viral particle sensing that can be adapted to other pathogens by simply changing the antibody added to the sample. Furthermore, by relying on this well-established linker system, incubation times and the stability of the linkage between the coated membrane and target are as optimal as could be expected. In this manner the µSIM-DX becomes modular, providing a consistent platform and pre-mix process where changes only need to be made to what the streptavidin conjugates to. It is also worth noting that affinity capture on the membrane seems irreversible as long as detergents are not added to the system. This would indicate that further test result analysis could be conducted on tested samples if necessary.
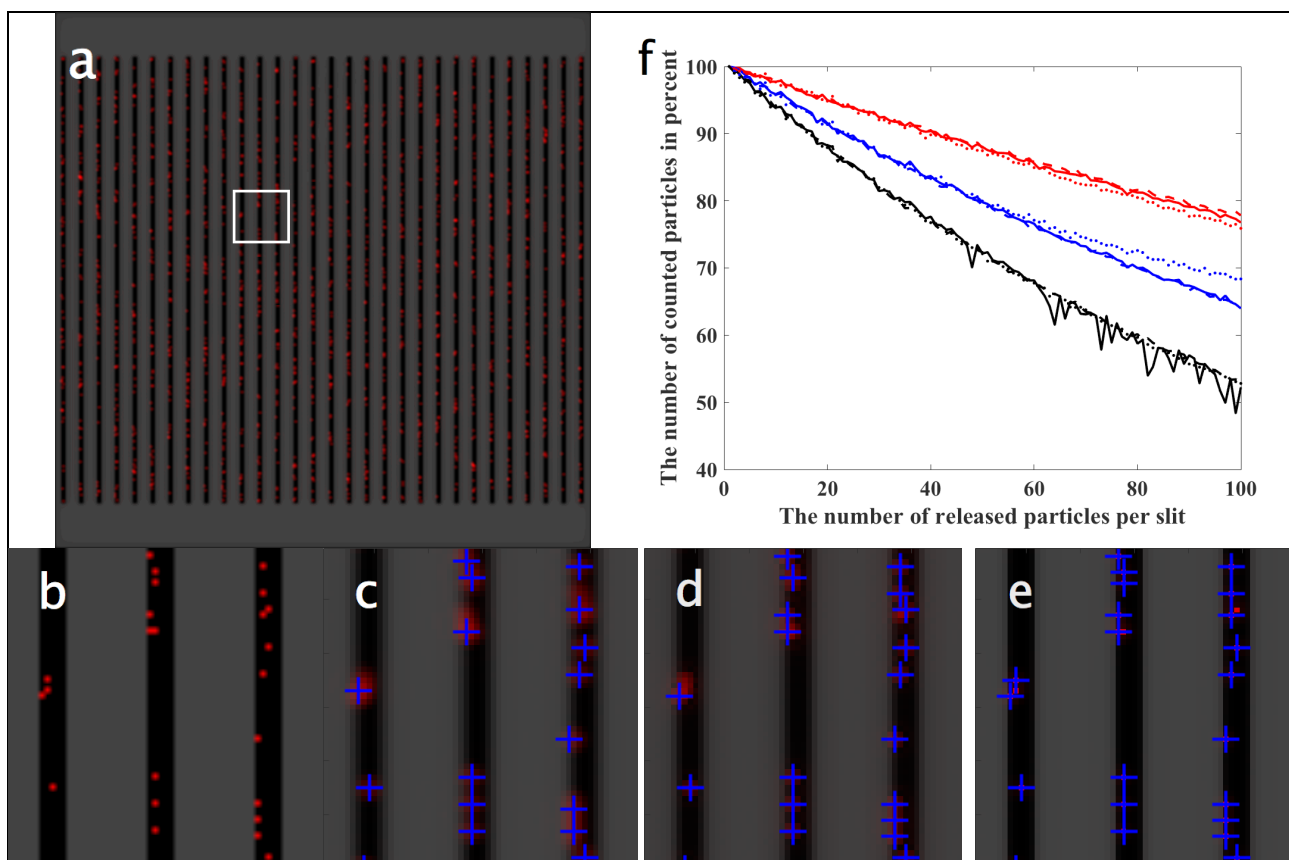
Figure 3. Synthetic (computer generated) wide-field nanomembrane image in full size (a), the cropped membrane scene (b), and the corresponding simulated wide-field (c), confocal (d), and STED (e) images. The counted particles are shown on the same figures using blue marker. The graph compares the number of released particles per slit and the number of counted particles in percent (f). The red, blue, and black colors correspond to STED, confocal, and wide-field microscope modalities, respectively. The solid, dashed, and dot lines indicate the particles of 100 nm, 200 nm, and 300 nm, respectively.

4.3 μSIM-DX specificity and sensitivity

The performance of the μSIM-DX relies on the design tolerances of its channels and the ability of the antibodies in the pre-mixing step to accurately bind to the correct target. Both aspects provide the device with its specificity and sensitivity. Since the resistance switch is tunable and is responsive to minute changes in channel resistances, consistency between device design is key to produce good specificity and sensitivity. Often, slight design differences lead to false positive results during our testing, lowering the device specificity. Sensitivity has been less of an issue, but cross reactivity of antibodies to similar species could pose a risk in the future. To maximize the specificity and sensitivity of the μSIM-DX sensors, design tolerances must be minimized and antibodies must be vetted carefully.

4.4 Counting accuracy and dose dependance

Counting simulated particle capture within the μSIM-DX has shown that it can be an effective means to quantify capture within the device. While only simulated images are counted in this paper, real images will be counted in the future. When interpreting the results of the counting experiments, it is interesting to note the dose dependance that the algorithm displays. Shown in the graph in Figure 3f, a trend is revealed where accuracy of the algorithm is directly tied to how many particles are released to the membrane. More particles means the chances that captured particles overlap is higher. This leads to error within the counting algorithm which is only alleviated by higher resolution imaging. For each imaging modality, noise/disparity in counting remains steady up until there are 45, 55, and 65 particles released per slit in wide-field, confocal, and STED respectively. This would mean that the upper limit of detection for counting in each modality over an entire membrane (25200 total pores) would be 1.1E6, 1.4E6, and 1.6E6 total released particles respectively. Based off of this, if

we maintain sample injections of less than 100 microliters, particle capture could be accurately quantified in solutions up to 1E8 particles/mL. While this could increase sample processing times in the future, the issue of overcrowding can be averted with serial dilution. After dilution, accurate particle counts can be completed which can be projected back up the dilution chain. This method will allow us to confirm that we have the sensitivity to determine whether or not an individual has an active infection of SARS-CoV-2.

5. CONCLUSIONS

Among the many POC diagnostics available, the μSIM-DX has the potential to provide new information about patient infection status. Specifically, because the sensor detects particles of a defined size with the proper surface antigen, the μSIM-DX should be sensitive to active infection and avoid the detection of viral fragments that have been associated with false positives[1-4,32]. The sensor design has been successfully developed into a working prototype, and the stable streptavidin-biotin linking system has been proven to work effectively after sample pre-mixing. Fluorescence microscopy was used to confirm sample capture, and simulation has shown the potential for fluorescence microscopy to provide a method of sample capture quantification. These developments target areas which need improvement within our current testing capabilities and show substantial potential to meet demand for more informative POC SARS-CoV-2 testing.

REFERENCES

[1] Lan, L., Xu, D., Ye, G., Xia, C., Wang, S., Li, Y. and Xu, H., "Positive RT-PCR Test Results in Patients Recovered from COVID-19," JAMA, 323(15), 1502-1503 (2020)

[2] Vargas-Ferrer, J. and Zamora-Mostacero, V., "Re-Detectable Positive RT-PCR Test Results in Recovered COVID-19 Patients: The Potential Role of ACE2," Disaster Medicine and Public Health Preparedness, 14(4), e36 (2020)

[3] An, J., Liao, X., Xiao, T., Qian, S., Yuan, J., Ye, H., Qi, F., Shen, C., Wang, L., Liu, Y., Cheng, X., Li, N., Cai, Q., Wang, F., Chen, J., Li, G., Cai, Q., Liu, Y., Wang, Y., Zhang, F., Fu, Y., He, Q., Tan, X., Liu, L. and Zhang, Z., "Clinical Characteristics of Recovered COVID-19 Patients with Re-Detectable Positive RNA Test," Annals of Translational Medicine, 8(17), 1084-1084 (2020)

[4] Cao, H., Ruan, L., Liu, J. and W. Liao, "The Clinical Characteristic of Eight Patients of COVID-19 with Positive RT-PCR Test After Discharge," Journal of Medical Virology, 92(10), 2159-2164 (2020)

[5] Özçürümez, M.K., Ambrosch, A., Frey, O., Haselmann, V., Holdenrieder, S., Kiehntopf, M., Neumaier, M., Walter, M., Wenzel, F., Wölfel, R., Renz, H. and COVID-19 Task Force of the German Society for Clinical Chemistry and Laboratory Medicine (DGKL), "SARS-CoV-2 Antibody testing—questions to be Asked," J. Allergy Clin. Immunol, 146 (1), 35-43 (2020).

[6] Sethuraman, N., Jeremiah, S.S. and Ryo, A., "Interpreting Diagnostic Tests for SARS-CoV-2," JAMA, 323(22), 2249-2251 (2020)

[7] Acuti Martellucci, C., Flacco, M.E., Cappadona, R., Bravi, F., Mantovani, L. and Manzoli, L., "SARS-CoV-2 pandemic: An overview," Advances in biological regulation, 77, 100736-100736 (2020)

[8] Zhai, P., Ding, Y., Wu, X., Long, J., Zhong, Y. and Li, Y., "The Epidemiology, Diagnosis and Treatment of COVID-19," International Journal of Antimicrobial Agents, 55(5), 105955-105955 (2020)

[9] Babiker, A., Myers, C.W., Hill, C.E. and Guarner, J., "SARS-CoV-2 Testing: Trials and Tribulations," Am. J. Clin. Pathol, 153(6), 706-708 (2020)

[10] " In Vitro Diagnostics EUAs," U.S. Food and Drug Administration, 28 January 2021, https://www-fda-gov.ezpminer.urmc.rochester.edu/medical-devices/coronavirus-disease-2019-covid-19-emergency-use-authorizations-medical-devices/vitro-diagnostics-euas (2020)

[11] Schermer, B., Fabretti, F., Damagnez, M., Di Cristanziano, V., Heger, E., Arjune, S., Tanner, N.A., Imhof, T., Koch, M., Ladha, A., Joung, J., Gootenberg, J.S., Abudayyeh, O.O., Burst, V., Zhang, F., Klein, F., Benzing, T. and Müller, R., "Rapid SARS-CoV-2 Testing in Primary Material Based on a Novel Multiplex RT-LAMP Assay." PloS One, 15(11), e0238612-e0238612 (2020)

[12] Baek, Y.H., Um, J., Antigua, K.J.C., Park, J., Kim, Y., Oh, S., Kim, Y., Choi, W., Kim, S.G., Jeong, J.H., Chin, B.S., Nicolas, H.D.G., Ahn, J., Shin, K.S., Choi, Y.K., Park, J. and Song, M., "Development of a Reverse Transcription-Loop-Mediated Isothermal Amplification as a Rapid Early-Detection Method for Novel SARS-CoV-2." Emerging Microbes & Infections, 9(1), 998-1007 (2020)

[13] Charlton, C.L., Kanji, J.N., Johal, K., Bailey, A., Plitt, S.S., MacDonald, C., Kunst, A., Buss, E., Burnes, L.E., Fonseca, K., Berenger, B.M., Schnabl, K., Hu, J., Stokes, W., Zelyas, N. and Tipples, G., "Evaluation of Six Commercial Mid- to High-Volume Antibody and Six Point-of-Care Lateral Flow Assays for Detection of SARS-CoV-2 Antibodies", J. Clin. Microbiol, 58(10), e01361-e013-20 (2020)

[14] Xie, X., Nielsen, M.C., Muruato, A.E., Fontes-Garfias, C.R. and Ren, P., "Evaluation of a SARS-CoV-2 lateral flow assay using the plaque reduction neutralization test," Diagnostic microbiology and infectious disease, 99(2), 115248-115248 (2021)

[15] Flower, B., Brown, J.C., Simmons, B., Moshe, M., Frise, R., Penn, R., Kugathasan, R., Petersen, C., Daunt, A., Ashby, D., Riley, S., Atchison, C.J., Taylor, G.P., Satkunarajah, S., Naar, L., Klaber, R., Badhan, A., Rosadas, C., Khan, M., Fernandez, N., Sureda-Vives, M., Cheeseman, H.M., O'Hara, J., Fontana, G., Pallett, S.J.C., Rayment, M., Jones, R., Moore, L.S.P., McClure, M.O., Cherepanov, P., Tedder, R., Ashrafian, H., Shattock, R., Ward, H., Darzi, A., Elliot, P., Barclay, W.S. and Cooke, G.S., "Clinical and laboratory evaluation of SARS-CoV-2 lateral flow assays for use in a national COVID-19 seroprevalence survey," Thorax, 75(12), 1082-1088 (2020)

[16] Michel, M., Bouam, A., Edouard, S., Fenollar, F., Di Pinto, F., Mège, J., Drancourt, M. and Vitte, J., "Evaluating ELISA, Immunofluorescence, and Lateral Flow Assay for SARS-CoV-2 Serologic Assays," Frontiers in microbiology, 11, 597529-597529 (2020)

[17] Boodman, C., Lagacé-Wiens, P. and Bullard, J., "Diagnostic Testing for SARS-CoV-2," CMAJ, 192(26), E713-E713 (2020)

[18] Bullard, J., Dust, K., Funk, D., Strong, J.E., Alexander, D., Garnett, L., Boodman, C., Bello, A., Hedley, A., Schiffman, Z., Doan, K., Bastien, N., Li, Y., Van Caeseele, P.G. and Poliquin, G., "Predicting Infectious Severe Acute Respiratory Syndrome Coronavirus 2 from Diagnostic Samples," Clinical Infectious Diseases, 71(10), 2663-2666 (2020)

[19] Striemer, C.C., Fauchet, P.M., Gaborski, T.R. and McGrath, J.L., "Charge- and Size-Based Separation of Macromolecules using Ultrathin Silicon Membranes," Nature, 445(7129), 749-753 (2007)

[20] Agrawal, A.A., Nehilla, B.J., Reisig, K.V., Gaborski, T.R., Fang, D.Z., Striemer, C.C., Fauchet, P.M. and McGrath, J.L., "Porous Nanocrystalline Silicon Membranes as Highly Permeable and Molecularly Thin Substrates for Cell Culture," Biomaterials, 31(20), 5408-5417 (2010)

[21] Gaborski, T.R., Snyder, J.L., Striemer, C.C., Fang, D.Z., Hoffman, M., Fauchet, P.M. and McGrath, J.L., "High-Performance Separation of Nanoparticles with Ultrathin Porous Nanocrystalline Silicon Membranes." ACS Nano, 4(11), 6973-6981 (2010)

[22] Salminen, A.T., Zhang, J., Madejski, G.R., Khire, T.S., Waugh, R.E., McGrath, J.L. and Gaborski, T.R., "Ultrathin Dual-Scale Nano- and Micro-Porous Membranes for Vascular Transmigration Models," Small, 15(6), e1804111-e1804111 (2019)

[23] Dehghani, M., Lucas, K., Flax, J., McGrath, J. & Gaborski, T., "Tangential Flow Microfluidics for the Capture and Release of Nanoparticles and Extracellular Vesicles on Conventional and Ultrathin Membranes," Advanced Materials Technologies, 4(11), 1900539, (2019)

[24] Masters, E.A., Salminen, A.T., Begolo, S., Luke, E.N., Barrett, S.C., Overby, C.T., Gill, A.L., de Mesy Bentley, Karen L, Awad, H.A., Gill, S.R., Schwarz, E.M. and McGrath, J.L., "An in Vitro Platform for Elucidating the Molecular Genetics of S. Aureus Invasion of the Osteocyte Lacuno-Canalicular Network during Chronic Osteomyelitis," Nanomedicine, 21, 102039-102039 (2019)

[25] Khire, T.S., Salminen, A.T., Swamy, H., Lucas, K.S., McCloskey, M.C., Ajalik, R.E., Chung, H.H., Gaborski, T.R., Waugh, R.E., Glading, A.J. and McGrath, J.L., "Microvascular Mimetics for the Study of Leukocyte-Endothelial Interactions," Cellular and Molecular Bioengineering, 13(2), 125 (2020)

[26] Winans, J.D., Smith, K.J.P., Gaborski, T.R., Roussie, J.A. and McGrath, J.L., "Membrane Capacity and Fouling Mechanisms for Ultrathin Nanomembranes in Dead-End Filtration," Journal of Membrane Science, 499, 282-289 (2016)

[27] Williams, E., Barr, K., Korchagina, E., Tuzikov, A., Henry, S. and Bovin, N., "Ultra-Fast Glyco-Coating of Non-Biological Surfaces," International Journal of Molecular Sciences, 17(1) 118 (2016)

[28] Henry, S., Williams, E., Barr, K., Korchagina, E., Tuzikov, A., Ilyushina, N., Abayzeed, S.A., Webb, K.F. and Bovin, N., "Rapid One-Step Biotinylation of Biological and Non-Biological Surfaces," Scientific Reports, 8(1), 2845-2846 (2018)

[29] Diamandis, E.P. and Christopoulos, T.K., "The Biotin-(Strept)Avidin System: Principles and Applications in Biotechnology," Clinical Chemistry, 37(5), 625 (1991)

[30] Locker, J.K., Kuehn, A., Schleich, S., Rutter, G., Hohenberg, H., Wepf, R. and Griffiths, G., "Entry of the Two Infectious Forms of Vaccinia Virus at the Plasma Membane is Signaling-Dependent for the IMV but Not the EEV," Molecular Biology of the Cell, 11(7), 2497-2511 (2000)

[31] Astuti, I. and Ysrafil, "Severe Acute Respiratory Syndrome Coronavirus 2 (SARS-CoV-2): An Overview of Viral Structure and Host Response," Diabetes & Metabolic Syndrome Clinical Research & Reviews, 14(4), 407-412 (2020)

[32] Molina, L.P., Chow, S., Nickel, A. and Love, J.E., "Prolonged Detection of Severe Acute Respiratory Syndrome Coronavirus 2 (SARS-CoV-2) RNA in an Obstetric Patient with Antibody Seroconversion," Obstetrics and Gynecology, 136(4), 838-841 (2020)